Earth and Planetary Science Letters 365 (2013) 38–50

Contents lists available at SciVerse ScienceDirect

Earth and Planetary Science Letters

journal homepage: www.elsevier.com/locate/epsl

Changes in Pacific Ocean circulation following the Miocene onset of permanent Antarctic ice cover

Ann Holbourn [a,*], Wolfgang Kuhnt [a], Martin Frank [b], Brian A. Haley [b,c]

[a] Institute of Geosciences, Christian-Albrechts University, D-24118 Kiel, Germany
[b] GEOMAR Helmholtz Centre for Ocean Research Kiel, D-24148 Kiel, Germany
[c] COAS Administration Building 104, Oregon State University, Corvallis, OR 97331-5503, USA

ARTICLE INFO

Article history:
Received 21 May 2012
Received in revised form
7 January 2013
Accepted 16 January 2013
Editor: G. Henderson

Keywords:
benthic stable isotopes
Nd isotopes
Pacific Ocean circulation
middle Miocene

ABSTRACT

We integrate micropaleontological and geochemical records (benthic stable isotopes, neodymium isotopes, benthic foraminiferal abundances and XRF-scanner derived elemental data) from well-dated Pacific Ocean successions (15–12.7 Ma) to monitor circulation changes during the middle Miocene transition into a colder climate mode with permanent Antarctic ice cover. Together with previously published records, our results show improvement in deep water ventilation and strengthening of the meridional overturning circulation following major ice expansion at ~13.9 Ma. Neodymium isotope data reveal, however, that the provenance of intermediate and deep water masses did not change markedly between 15 and 12.7 Ma. We attribute the increased $\delta^{13}C$ gradient between Pacific deep and intermediate water masses between ~13.6 and 12.7 Ma to more vigorous entrainment of Pacific Central Water into the wind-driven ocean circulation due to enhanced production of intermediate and deep waters in the Southern Ocean. Prominent 100 kyr ventilation cycles after 13.9 Ma reveal that the deep Pacific remained poorly ventilated during warmer intervals at high eccentricity, whereas colder periods (low eccentricity) were characterized by a more vigorous meridional overturning circulation with enhanced carbonate preservation. The long-term $\delta^{13}C$ decline in Pacific intermediate and deep water sites between 13.5 and 12.7 Ma reflects a global trend, probably related to a re-adjustment response of the global carbon cycle following the last 400 kyr carbon maximum (CM6) of the "Monterey Excursion".

1. Introduction

The meridional overturning circulation (MOC) plays a key role in regulating global climate, as it strongly influences CO_2 storage in the deep ocean, latitudinal heat transport and gas exchange with the atmosphere. The ocean's density structure and the strength of the MOC are largely controlled by the source and rate of deep and intermediate water production. Thus, reconstructing past water mass distribution and changes in ocean circulation is critical for understanding long-term climate development and the processes driving climate change, as well as for predicting future trends. Comparatively little is known about the evolution of intermediate and deep water masses and the development of ocean circulation during the middle Miocene, when Earth's climate transitioned from relatively warm conditions ("Miocene Climatic Optimum") into a colder mode, characterized by permanent polar ice cover following Antarctic ice-sheet expansion.

Changes in the configuration of low latitude inter-oceanic passages altering water exchange and heat fluxes between the Pacific and Atlantic Oceans (Central American Seaway) and between the Tethys, Indian and Southern Oceans (eastern portal of Tethys Ocean) have been conjectured as the main drivers of long-term Miocene climate and oceanographic evolution (Woodruff and Savin, 1989; Wright et al., 1992; Heinze and Crowley, 1997; Nisancioglu et al., 2003; Motoi et al., 2005; von der Heydt and Dijkstra, 2006; Butzin et al., 2011). However, results from modeling experiments appear somewhat contradictory, and paleoceanographic reconstructions, based on paleontological and geochemical proxy data, are often poorly constrained, thus providing limited insights into the main processes controlling ocean circulation during middle Miocene warmer and cooler phases. In particular, the source of deep water formation and changing rates of the MOC on a warmer Earth without a fully developed Antarctic ice sheet remain matters of intense debate. These issues are specifically relevant to constrain contrasting scenarios of future climate evolution. Thus, the warmer middle Miocene period potentially provides a useful analog to test predicted changes in ocean circulation associated with global warming and melting of polar ice.

A major challenge for paleoceanographic and paleoclimate reconstructions that extend beyond the Pleistocene and Pliocene is that continuous, well-preserved marine sedimentary records are sparse and age models have large uncertainties. Here, we

* Corresponding author. Tel.: +49 4318802938.
E-mail address: ah@gpi.uni-kiel.de (A. Holbourn).

0012-821X/$ - see front matter © 2013 Elsevier B.V. All rights reserved.
http://dx.doi.org/10.1016/j.epsl.2013.01.020

compare ventilation and water mass proxy data (benthic $\delta^{18}O$ and $\delta^{13}C$, radiogenic Nd isotopes, benthic foraminiferal distribution and XRF scanning Mn/Ca data) in well-dated, expanded sedimentary sequences from Pacific sites sampling different intermediate to deep water masses. We focus on the middle Miocene interval from 15 to 12.7 Ma, which includes the major Antarctic ice sheet expansion and global cooling step at ~13.9 Ma (Shackleton and Kennett, 1975; Savin et al., 1975; Woodruff and Savin, 1991; Wright et al., 1992; Flower and Kennett, 1993, 1995; Abels et al., 2005; Holbourn et al., 2005, 2007; Shevenell et al., 2004, 2008). Integration of new and published data sets from Southeast Pacific Ocean Drilling Program (ODP) Sites 1236 and 1237, western Equatorial Pacific ODP Site 806, central Equatorial Pacific Deep Sea Drilling Program (DSDP) Site 574, Southwest Pacific DSDP Sites 588 and 590, and Southern Ocean ODP Site 1171 allows to closely monitor water mass evolution and changes in the strength of the Pacific MOC following the major Antarctic ice sheet expansion marking the end of the middle Miocene warm period.

2. Pacific Ocean circulation

2.1. Modern oceanography

Today, the deep Pacific basin is mainly fed by Circumpolar Deep Water (CPDW), a mixture of Antarctic Bottom Water (AABW) and North Atlantic Deep Water (NADW) that originates from the Antarctic Circumpolar Current (Reid, 1986, 1997; Talley, 1993; Tsuchiya and Talley, 1996; Sigman et al., 2010). This deep water accumulates nutrients and loses oxygen as it transits northwards into the North Pacific before returning as a nutrient enriched, oxygen depleted southward flow (Pacific Central Water, PCW) at 1–3 km depth (Fig. 1). Deep water is not formed in the open North Pacific Ocean presently due to low salinity surface waters inhibiting convection (Warren, 1983; Emile-Geay et al., 2003; Kiefer, 2010). Pacific intermediate waters, which have their sources in the Southern as well as the Northern Hemispheres, exhibit highly contrasting properties (Fig. 1). The Antarctic Intermediate Water (AAIW) is a nutrient depleted water mass with high oxygen content and a high $\delta^{13}C$ signature that extends to ~15–20°S in the South Pacific Ocean and is centered at water depths of 800–1000 m (Kroopnick, 1985; Tsuchiya and Talley, 1996; Talley, 1999). The North Pacific Intermediate Water (NPIW), which originates in the northwest Pacific Ocean, spreads south to latitudes of 15–20°N in water depths of 400–700 m (Talley, 1993, 1997; You, 2003). In contrast to the AAIW, the NPIW forms with relatively little contact to the atmosphere and is thus characterized by abundant nutrients, low oxygen content and low $\delta^{13}C$ values. Radiocarbon ages from the North Pacific, Atlantic and Southern Oceans revealed that deep water ventilation changed markedly over the last glacial cycle (Sikes et al., 2000; Robinson et al., 2005; Galbraith et al., 2007; Marchitto et al., 2007), although patterns are more equivocal in other regions of the Pacific Ocean (Broecker et al., 2004, 2008). In the North Pacific and Atlantic Oceans, there is evidence that the abyssal ocean remained poorly ventilated during the Last Glacial Maximum and early deglaciation until vigorous NADW formation resumed at ~14.6 ka (Galbraith et al., 2007). This led to the suggestion that enhanced NADW formation near the start of the Bølling promoted an increased

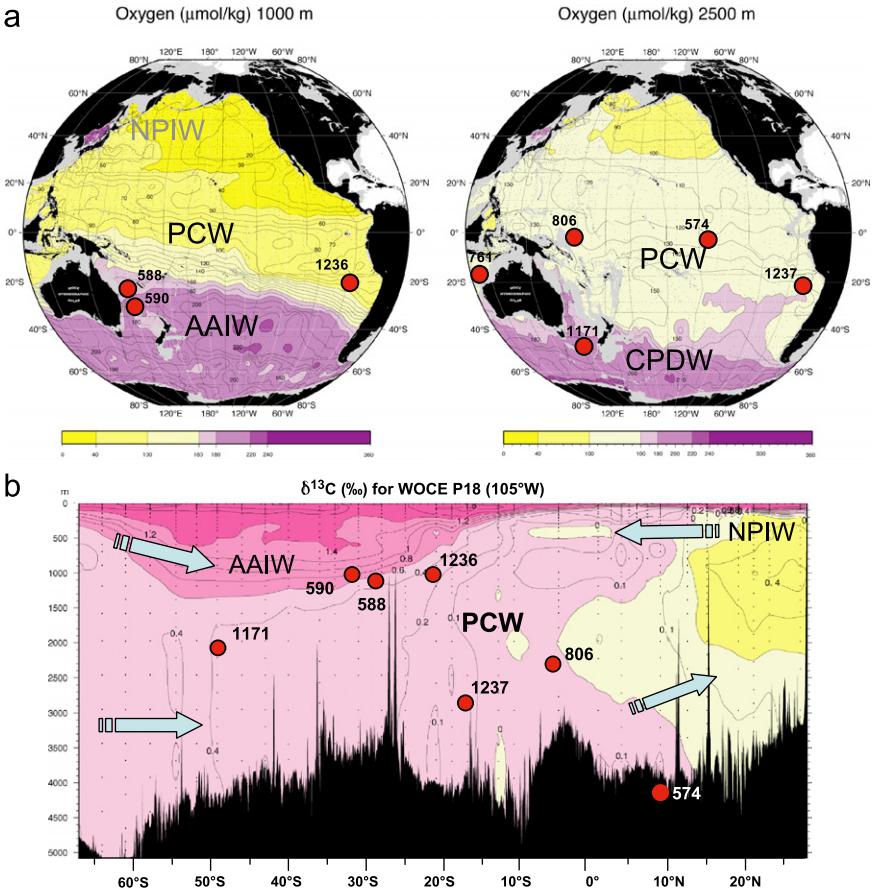

Fig. 1. (a) Modern O_2 distribution at 1000 m and 2500 m water depth in Pacific Ocean (Talley, 2007) and (b) vertical profile showing present day distribution of water masses in Pacific Ocean with locations of ODP Sites 1236 and 1237 and $\delta^{13}C$ (WOCE, Talley, 2007). NPIW: North Pacific Intermediate Water, PCW: Pacific Central Water, AAIW: Antarctic Intermediate Water, CPDW: Circumpolar Deep Water. Locations of sites discussed in text are shown.

flux of deep waters from the South into the Pacific Ocean, stimulating entrainment of deep waters into the wind-driven circulation and leading to a rapid improvement in deep water ventilation (Galbraith et al., 2007).

2.2. Middle Miocene paleoceanography

The composition and distribution of Pacific water masses and inter-ocean circulation patterns during the Neogene are still poorly known. Comparison of benthic carbon and oxygen isotope data from the Atlantic, Indian, Pacific and Southern Oceans initially provided evidence that the Southern Ocean was the dominant source of deep water through the middle Miocene, whereas NADW formation remained weak until ~12.5 Ma (Woodruff and Savin, 1989, 1991; Wright et al., 1992; Wright and Miller, 1993). Inter-basin gradients also suggested that a low latitude source of warm, saline deep water in the northern Indian Ocean or Tethys Ocean terminated at ~15 Ma due to closure of the eastern portal of the Tethys Ocean (Woodruff and Savin, 1989; Wright et al., 1992). Stable isotope data additionally indicated maximum production of southern component intermediate waters as well as increased influence of PCW in the Southwest Pacific Ocean after 13.6 Ma following major ice expansion in East Antarctica (Flower and Kennett, 1995).

The most recent benthic $\delta^{13}C$ compilations from multiple ocean sites support relatively small inter-basin gradients until ~12 Ma (Poore et al., 2006) or ~13 Ma (Cramer et al., 2009), pointing to a common source for deep water formation in the Southern Ocean over the early and middle Miocene. These findings were corroborated by Nd isotope studies of ferromanganese crusts from Equatorial and Southwest Pacific deep waters that indicated increasing export of Southern Ocean deep water to the Pacific Ocean over the Neogene (van de Flierdt et al., 2004a). Modeling experiments additionally suggested that North Atlantic deep water formation did not occur or remained relatively weak until the late Miocene (Butzin et al., 2011), in agreement with Nd isotope data indicating onset of NADW formation between 10.6 and 7.3 Ma (Thomas and Via, 2007). However, these results contrast with interpretations of Nd isotope time series from the Atlantic Ocean suggesting that continuous export of NADW may have started as early as 14 Ma (Frank et al., 2002). Recent studies, based on Nd isotopes and inter-ocean $\delta^{13}C$ gradients, provided evidence for an even earlier beginning of NADW export in the early Oligocene (Via and Thomas, 2006; Scher and Martin, 2008; Katz et al., 2011).

3. Site locations

ODP Sites 1236 (21°21.539′S, 81°26.165′W; 1323 m water depth) and 1237 (16°0.421′S, 76°22.685′W; 3212 m water depth) on the Nazca Ridge are ideally located to document past variations of intermediate and deep water masses in the subtropical Southeast Pacific Ocean (Fig. 1). Tectonic backtracking to shallower depths suggests that deeper Site 1237 was bathed in PCW (or its paleoequivalent), whereas the shallower Site 1236 was also influenced by AAIW (or its paleoequivalent) during the Miocene (Mix et al., 2003). The backtracking paths move Sites 1236 and 1237 ~20° westward relative to South America over the last 25 Myr (Mix et al., 2003). During the middle Miocene, both sites were located ~10° westward of their present positions in an oligotrophic region of the subtropical gyre still relatively far from the productive upwelling systems of Peru (Mix et al., 2003). Middle Miocene sediments recovered with the Advanced Piston Corer system consist of unlithified, white to pale brown nannofossil oozes with an average of 95 wt% calcium carbonate (Mix et al., 2003). Average sedimentation rates over the middle Miocene at these two sites are ~1 cm/kyr.

To better understand the distribution of water masses in the Pacific Ocean during the middle Miocene, we integrated the 1236 and 1237 records with new and published benthic isotope and radiogenic Nd isotope data from DSDP Sites 574, 588, 590 and ODP Sites 761, 806, 1171 (a summary of site locations and data sets discussed in this work is provided in Table 1). ODP Site 806 (0°19.11′N, 159°21.69′E; 2520 m water depth) was selected to monitor changes in the properties of western Equatorial Pacific deep water. Middle Miocene sediments at this relatively deep location consist of foraminifer nannofossil chalks with a carbonate content of 90–95 wt% (Kroenke et al., 1991). ODP Site 574 (04° 12.52′N, 133° 19.81′W; 4561 m water depth) recovered a sequence of middle Miocene calcareous ooze chalks with a carbonate content of 90–95 wt% from the abyssal central Equatorial Pacific Ocean (Mayer et al., 1985). Sediments are unusually well preserved at this location, which remained above the lysocline during the middle Miocene and did not become deeply buried subsequently. DSDP Site 588 (26°06.7′S, 161°13.61′E;

Table 1
Summary of ODP/DSDP locations and data sets discussed in text.

DSDP/ODP Site	Latitude	Longitude	Water depth (m)	Location	Data sets	Reference
1236	21°21.539′S	81°26.165′W	1323	Nazca Ridge Southeast Pacific	Benthic foraminiferal stable isotopes	This work
					Nd isotopes	This work
1237	16°0.421′S	76°22.685′W	3212	Nazca Ridge Southeast Pacific	Benthic foraminiferal stable isotopes	Holbourn et al. (2005, 2007)
					Nd isotopes	This work
					Benthic foraminiferal census counts	This work
					XRF log(Mn/Ca)	Holbourn et al. (2005, 2007) and this work
1171	48°29.9971′S	149°6.7051′E	2150	South Tasman Rise Southern Ocean	Benthic foraminiferal stable isotopes	Shevenell et al. (2004, 2008)
					Nd isotopes	This work
806	0°19.11′N	159°21.69′E	2520	Ontong Java Plateau Western Equatorial Pacific	Benthic foraminiferal stable isotopes	This work
					Nd isotopes	This work
761	16°44.23′S	115°32.10′E	2189	Wombat Plateau Eastern Indian Ocean	Nd isotopes	This work
574	4°12.52′N	133°19.81′W	4561	Central Equatorial Pacific	Benthic foraminiferal stable isotopes	Pisias et al. (1985)
588	26°06.7′S	161°13.61′E	1533	Lord How Rise Southwest Pacific	Benthic foraminiferal stable isotopes	Flower and Kennett (1995)
590	31°10.02′S	163°21.51′E	1299	Lord How Rise Southwest Pacific	Benthic foraminiferal stable isotopes	Flower and Kennett (1995)

1533 m water depth), Site 590 (31°10.02′S, 163°21.51′E; 1299 m water depth), and Site 591 (31°35.06′S, 164°26.92′E; 2131 m water depth) form a depth transect on the Lord Howe Rise in the Southwest Pacific Ocean, allowing reconstruction of vertical water mass structure and circulation development. These sites were situated ~4° South of their present location and in comparable water depths during the middle Miocene (Flower and Kennett, 1995). ODP Site 1171 (48°29.9971′S, 149°6.7051′E; 2150 m water depth), located at paleolatitudes of 55°S and in paleodepths of ~1600 m during the middle Miocene, provides insights into the properties of CPDW or "Southern Component Water" (Shevenell et al., 2008). ODP Site 761 (16°44.23′S, 115°32.10′E; 2189 m water depth), located on the Wombat Plateau off northwestern Australia, is included for comparison with the eastern subtropical Indian Ocean.

4. Methods

4.1. Stable isotope analysis (ODP Sites 806 and 1236)

Nannofossil chalks in Hole 806B were sampled at ~20 cm intervals (~5–6 kyr resolution, 20 cm^3 sample size) between 455.95 and 498.85 mbsf. Nannofossil oozes in Site 1236 were sampled at ~4 cm intervals (~7 kyr resolution, 20 cm^3 sample size) from a composite sequence (the so-called splice) in Holes 1236B and C (77.66–96.73 m composite depth). All samples were oven dried at 40 °C and weighed before washing over a 63 μm sieve. Residues were oven dried at 40 °C on a sheet of filter paper, then weighed and sieved into different size fractions. We measured $\delta^{18}O$ and $\delta^{13}C$ in epifaunal benthic foraminifers >250 μm (*Cibicidoides wuellerstorfi* or/and *Cibicidoides mundulus*). Paired measurements in middle Miocene samples from ODP Sites 1146 and 1237 previously indicated no significant offset in $\delta^{18}O$ and $\delta^{13}C$ between *C. wuellerstorfi* and *C. mundulus* (Holbourn et al., 2007). Four to seven well-preserved tests were broken into large fragments, cleaned in alcohol in an ultrasonic bath, and were then dried at 40 °C. In a few samples with low foraminiferal abundances, only 1–3 specimens were analyzed. Measurements were made with the Finnigan MAT 251 mass spectrometer at the Leibniz Laboratory, Kiel University. The instrument is coupled on-line to a Carbo-Kiel Device (Type I). Samples were reacted by individual acid addition (99% H_3PO_4 at 73 °C). Standard external error is better than ±0.07‰ and ±0.05‰ for $\delta^{18}O$ and $\delta^{13}C$, respectively. Results were calibrated using the National Institute of Standards and Technology (Gaithersburg, Maryland) carbonate isotope standard NBS 20 and NBS 19 and 18, and are reported on the PeeDee belemnite (PDB) scale. A plot of the 1236 $\delta^{18}O$ record versus depth is shown in Fig. 2. Data sets are archived at WDC-MARE (http://www.pangaea.de).

4.2. Radiogenic Nd isotope analysis (ODP Sites 761, 806, 1171, 1236 and 1237)

The Nd isotope composition of past deep waters was extracted from bulk sediment samples by leaching of the ferromanganese coatings (Rutberg et al., 2000; Bayon et al., 2002; Piotrowski et al., 2005; Gutjahr et al., 2007). We applied the slightly modified

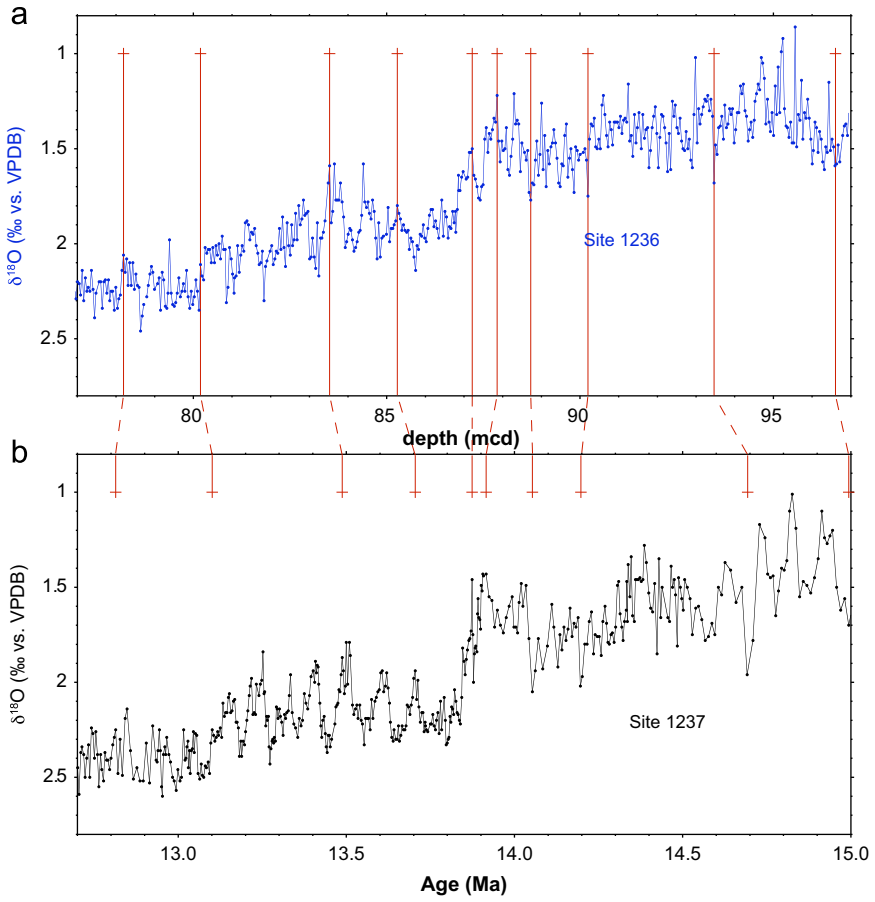

Fig. 2. (a) Benthic foraminiferal $\delta^{18}O$ profile plotted against composite depth in ODP Site 1236; (b) Orbitally-tuned benthic foraminiferal $\delta^{18}O$ series in ODP Site 1237 (Holbourn et al., 2005, 2007). Red crosses indicate tie points used to derive new age model for ODP Site 1236. (For interpretation of the references to color in this figure legend, the reader is referred to the web version of this article.)

method of Gutjahr et al. (2007), omitting the $MgCl_2$ leaching step to remove adsorbed metals before leaching of the coatings, as this step proved unnecessary. There is an ongoing discussion as to the reliability of these methods to extract a pure seawater Nd isotope signature (e.g. Roberts et al., 2009; Martin et al., 2010; Elmore et al., 2011). Martin et al. (2010) have demonstrated for several sites that the leached Nd isotope signatures agree well with fish teeth data, which provide robust records of seawater Nd (Martin and Scher, 2004). In addition, the Sr isotope composition of the leaches (after carbonate removal) matches the expected seawater data perfectly, which together suggests that our data reliably represent past seawater compositions.

For this study the dry and coarsely ground bulk sediments (1–2 g) were rinsed twice with de-ionized water (from a Milli-Q system). The carbonate fraction was dissolved and removed using a 15%-acetic acid/1 M-Na acetate buffer followed by a triple rinse with de-ionized water. The Fe–Mn oxide coatings were leached for 1 h in an ultrasonic bath and for 2 h in a shaker using a 0.05 M-hydroxylamine hydrochloride/15%-acetic acid solution buffered to pH 3.6 with NaOH. Separation and purification of Nd in the leachates and the dissolved detritus followed previously published standard procedures (Cohen et al., 1988; Barrat et al., 1996; Le Fèvre and Pin, 2005). Having separated Pb for a different study on anion exchange columns (50 µl AG1-X8 resin, mesh 100–200), the alkaline elements were separated from the rare earth elements on cation exchange columns (0.8 ml AG50W-X12 resin, mesh 200–400). Finally, Nd was separated from the other REEs on columns containing 2 ml Ln Spec resin (mesh 50–100).

The Nd isotope compositions were measured on a TIMS Triton at GEOMAR, Kiel. All $^{143}Nd/^{144}Nd$ ratios were mass bias corrected to $^{146}Nd/^{144}Nd=0.7219$ and normalized to the accepted value of the JNdi-1 standard of 0.512115 (Tanaka et al., 2000). The $^{143}Nd/^{144}Nd$ data are expressed as ε_{Nd} values, which corresponds to the deviation of the measured $^{143}Nd/^{144}Nd$ of the samples from CHUR (Chondritic Uniform Reservoir with $^{143}Nd/^{144}Nd=0.512638$, Jacobsen and Wasserburg, 1980) in parts per 10,000: $\varepsilon_{Nd}=[(^{143}Nd/^{144}Nd_{sample}/^{143}Nd/^{144}Nd_{CHUR})-1]\times 10.000$. Repeated measurements of the JNdi-1 standard over a period of several months gave a long-term reproducibility of ± 0.35 ε_{Nd} (2σ). Procedural Nd blanks were ≤ 25 pg.

4.3. XRF scanning (ODP Site 1237)

We performed x-ray fluorescence measurements with 1 cm resolution on the archive halves of the Site 1237 splice using the Cortex XRF-Scanner at the Bremen IODP Core Repository (X-ray voltage: 20 kV, 30 s count time, X-ray current: 0.087 mA). Overlapping measurements (50–100 cm) were made at correlation points between adjacent holes to verify the accuracy and completeness of the splice. We interpreted Mn maxima as intervals of increased carbonate dissolution caused by poor deep water ventilation and not as intervals of increased terrigenous dust flux or river runoff, based on co-variance of Fe and Mn, and the lack of co-variance of Fe and Mn with Ti (Holbourn et al., 2005, 2007).

4.4. Benthic foraminifers (ODP Site 1237)

Benthic foraminifers were picked and counted in the size fraction >250 µm from 282 samples (10 or 20 cm intervals) in Site 1237. Numbers of benthic foraminifers picked per sample generally vary between 50 and 250 (average of 93), except in rare samples in the lower part of the succession, where foraminiferal abundance was low and fewer specimens were picked. We used the total number of specimens and the number of *Cibicidoides* spp. per gram of dry sediment to monitor organic export fluxes and ventilation changes at the seafloor.

4.5. Chronologies

An orbitally-tuned chronology is available for the middle Miocene interval of Site 1237 (Holbourn et al., 2005, 2007) based on correlation of benthic $\delta^{18}O$ and XRF-derived Fe concentration data to computed variations of the Earth's orbit and solar insolation (obliquity and eccentricity in Laskar et al. (2004)). The Site 1236 shipboard age model had originally been constrained by eight biostratigraphic and five magnetostratigraphic datums over the middle Miocene interval (Mix et al., 2003). The shipboard age models for Sites 574 and 806 had initially been based on biostratigraphic datums (Mayer et al., 1985; Pisias et al., 1985; Kroenke et al., 1991). Chronologies over the middle Miocene interval had been previously developed for Sites 588 and 590 using biostratigraphic and isotopic datums as well as sedimentological information (Flower and Kennett, 1995).

We developed new chronologies by correlating the benthic $\delta^{18}O$ profiles in Sites 806 and 1236 and the published $\delta^{18}O$ data from Site 574 (Pisias et al., 1985) and Site 590 (Flower and Kennett, 1995) to the orbitally-tuned $\delta^{18}O$ series in Site 1237 (Fig. 2). Following this tuning procedure, we noted that the $\delta^{13}C$ records in Sites 574, 590, 806 and 1236 also showed a reasonably good match with the 1237 $\delta^{13}C$ profile, thus supporting the new age models derived from correlation of benthic $\delta^{18}O$ records (Figs. 3 and 4). For Sites 588, 761 and 1171, we used revised chronologies from Holbourn et al. (2004, 2007).

5. Nd isotopic composition of Pacific water masses

Our middle Miocene deep water Nd isotope data from multiple sites (Fig. 5) indicate that the signatures of Pacific end member water masses did not differ markedly from the present day in agreement with published data for the modern Pacific Ocean (Piepgras and Jacobsen, 1988; Lacan and Jeandel, 2001; Amakawa et al., 2009; Grasse et al., 2012) and Southern Ocean seawater (Stichel et al., 2012; Carter et al., 2012), fish teeth in surface sediments (Horikawa et al., 2011), and Fe–Mn crust surfaces (Albarède and Goldstein, 1992; Albarède et al., 1997; Frank, 2002), as well as Miocene Fe–Mn crusts and fish teeth (Ling et al., 1997, 2005; Frank et al., 1999, 2002; van de Flierdt et al., 2004a,b; see also Table DR1 in Newkirk and Martin (2009)). CPDW (Southern Component Water, Site 1171) has an ε_{Nd} value of -8 to -9, which is comparable to the modern and Miocene signatures of AAIW and CPDW in the Pacific and Atlantic sectors of the Southern Ocean. Further north in the subtropical Southeast Pacific Ocean, ε_{Nd} values of -3.5 to -5 for shallower Site 1236 and of -3 to -4 for the deeper Site 1237 are within the range of contemporary and Miocene PCW. In the western Equatorial Pacific Ocean (Site 806), the Nd isotopic composition varied mainly between $\varepsilon_{Nd}=-4.5$ and -3, which is also compatible with that of modern and Miocene PCW. Miocene ε_{Nd} signatures of -8 to -7 at Site 761 in the eastern subtropical Indian Ocean are close to present day values.

Thus, middle Miocene deep water Nd isotope signatures became progressively more radiogenic northward in the Pacific Ocean, mainly reflecting, as today, mixing of southern sourced waters with more radiogenic waters of northern origin. An influence by continental contributions in the western Pacific cannot be excluded (Horikawa et al., 2011) but was most likely small given the internal consistency of the data and the good correspondence with the present day distributions. The higher resolution records of Sites 1236 and 1237 located in different water depths (1323 m versus 3212 m, respectively) in the subtropical Southeast Pacific Ocean reveal no fundamental or persistent change in the mixtures of intermediate and deep subtropical water masses over the interval 15–12.7 Ma, encompassing the middle Miocene glacial expansion in Antarctica. Advection of AAIW can explain the overall less radiogenic Nd isotope composition at the shallower Site 1236, whereas the deeper Site 1237 remained

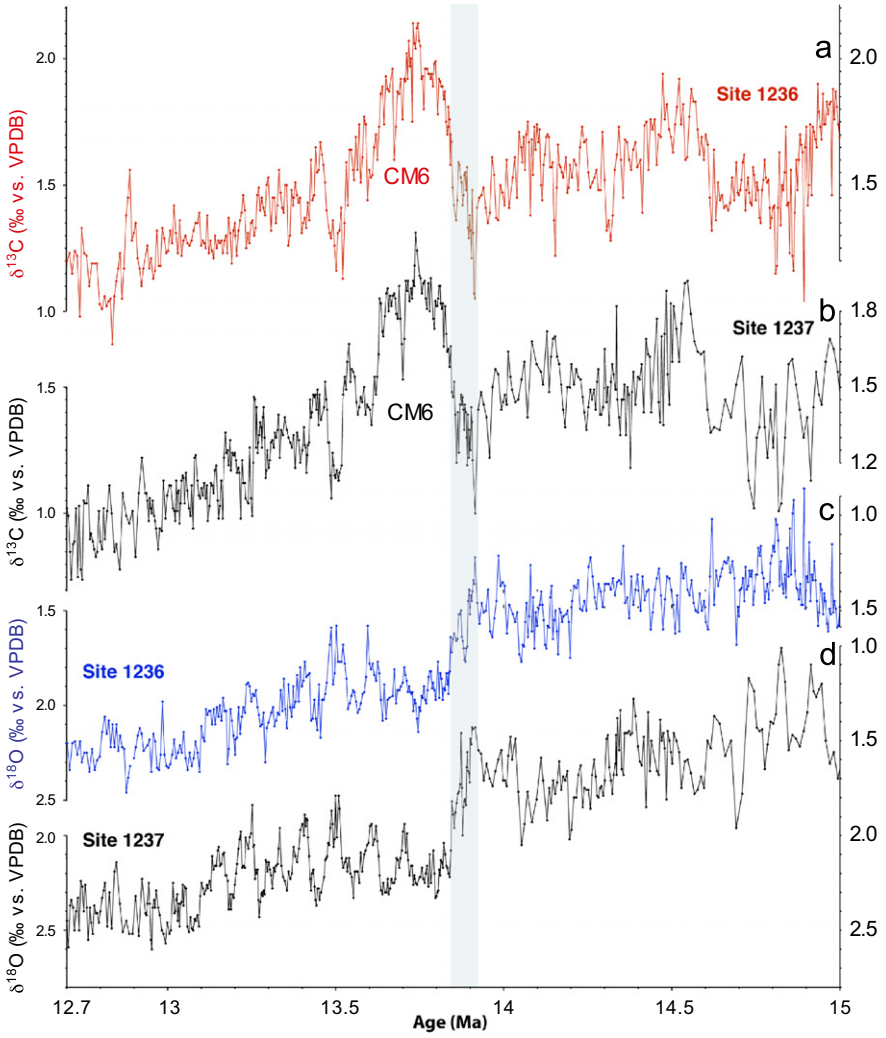

Fig. 3. (a–b) High-resolution benthic $\delta^{13}C$ records from ODP Sites 1236 (1323 m water depth) and 1237 (3212 m water depth) in the subtropical Southeast Pacific spanning the middle Miocene glacial expansion. CM6 indicates the last and most prominent $\delta^{13}C$ maximum of the "Monterey Excursion"; (c–d) Benthic $\delta^{18}O$ records from ODP Sites 1236 and 1237.

more influenced by the return flow of PCW. Between 14.3 and 13.6 Ma, Nd values in Sites 1236, 1237 and 806 are almost identical, implying that a homogenous water mass prevailed through the subtropical Southwest and Southeast Pacific (Fig. 5).

6. Southeast Pacific circulation

6.1. Intermediate water $\delta^{18}O$ and $\delta^{13}C$ (Site 1236)

The benthic $\delta^{18}O$ record from Site 1236 indicates recovery of a complete middle Miocene succession over the interval 15–12.7 Ma. The $\delta^{18}O$ time series displays characteristic features of high resolution middle Miocene $\delta^{18}O$ curves over this time interval (Shevenell and Kennett, 2004; Shevenell et al., 2004, 2008; Holbourn et al., 2005, 2007), including the major increase after 13.9 Ma (~0.8‰) associated with Antarctic ice sheet expansion (Fig. 3). Between ~14.1 and 13.9 Ma, the distinctive $\delta^{18}O$ minima preceding the major $\delta^{18}O$ shift are also clearly identifiable. The amplitude of $\delta^{18}O$ variations in Site 1236 is overall comparable or slightly lower (by <0.1‰) than at substantially deeper Site 1237, indicating that deep and intermediate water temperatures closely co-varied (Figs. 3 and 4). However, at shallower Site 1236 the $\delta^{18}O$ values are lower by 0.2–0.3‰ reflecting higher temperatures and/or lower salinity of intermediate waters.

The 1236 benthic $\delta^{13}C$ record is characterized by high-frequency variations (41 and 100 kyr periods), superimposed on lower frequency (400 kyr period) oscillations that exhibit a high degree of coherence with the $\delta^{13}C$ signal of the deeper Site 1237 (Fig. 3). Most prominent are the successive ~400 kyr cycles between 15 and 13.5 Ma with $\delta^{13}C$ maxima reaching ~1.7–2‰. These long-term $\delta^{13}C$ fluctuations represent the last four main cycles of the "Monterey Excursion". The last of the $\delta^{13}C$ maxima (CM6) shows the highest rate of increase within the "Monterey Excursion" and its onset coincides with the prominent $\delta^{18}O$ increase, associated with Antarctic glacial expansion after 13.9 Ma. A distinctive feature, when comparing the long-term evolution of the 1236 and 1237 curves, is the progressive offset that developed between the $\delta^{13}C$ signals after 13.6 Ma (Figs. 4–6). The intermediate (Site 1236) to deep (Site 1237) $\delta^{13}C$ gradient reached ~0.5‰ at 12.7 Ma, as $\delta^{13}C$ became increasingly more depleted at Site 1237, indicating either an improvement in intermediate water ventilation or changes in the preformed $\delta^{13}C$ signature of intermediate or/and deep water masses.

6.2. Deep water ventilation (Site 1237)

At the deeper Site 1237, located at a paleodepth close to the lysocline, the XRF Log(Mn/Ca) data, a proxy record for carbonate dissolution and deep water ventilation (Holbourn et al., 2005,

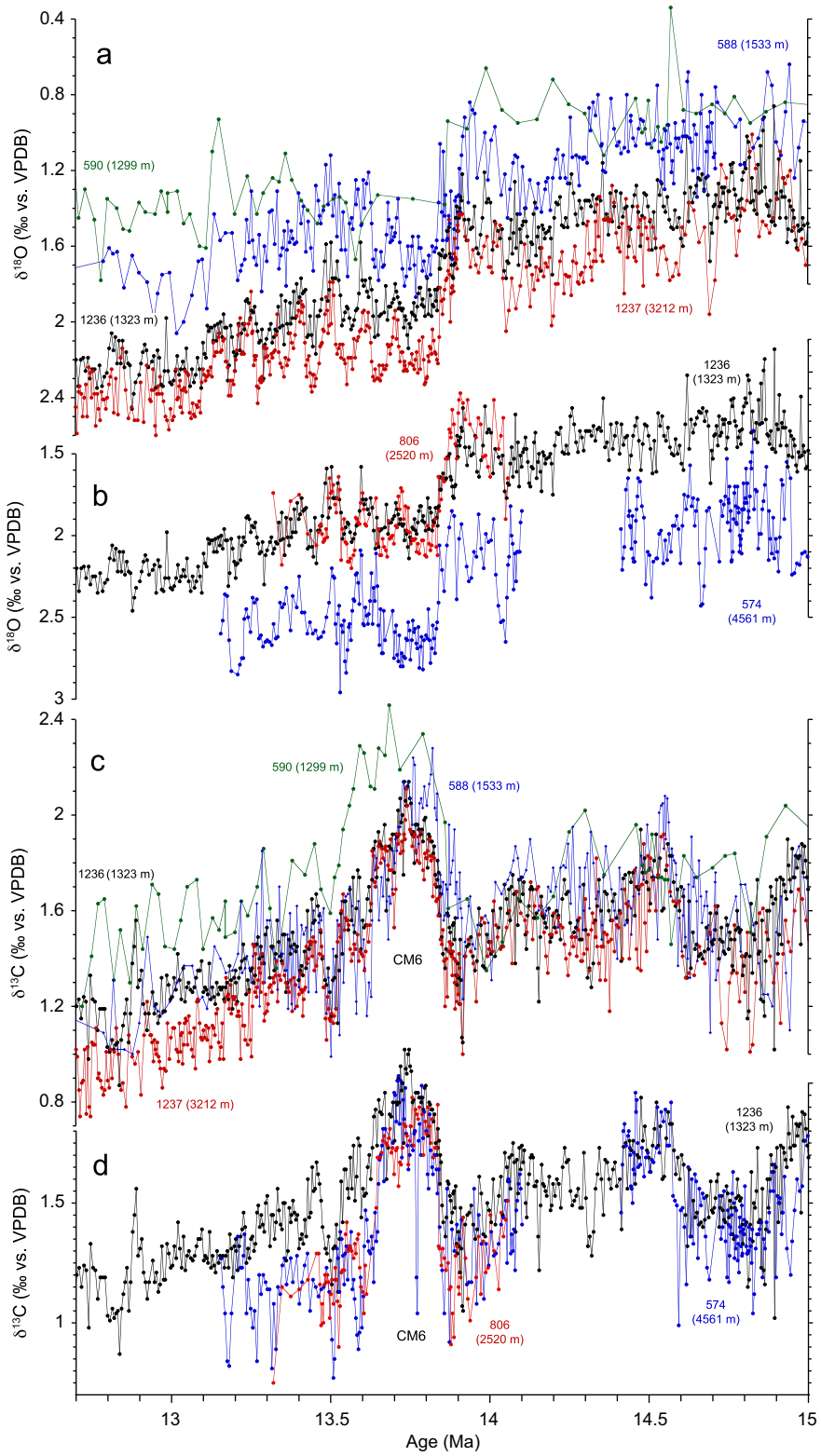

Fig. 4. (a) Comparison of δ^{18}O profiles in Southwest Pacific DSDP Sites 588 and 590 (Flower and Kennett, 1995) and Southeast Pacific ODP Sites 1236 and 1237; (b) comparison of δ^{18}O profiles in central Equatorial Pacific DSDP Site 574 (*C. wuellerstorfi* and *C. mundulus* values normalized to *Uvigerina* spp. values by a correction of 0.64‰ for *C. wuellerstorfi* and 0.50‰ for *C. mundulus* from Pisias et al. (1985)), western Equatorial Pacific ODP Site 806 and Southeast Pacific ODP Site 1236; (c) comparison of δ^{13}C profiles in Southwest Pacific DSDP Sites 588 and 590 (Flower and Kennett, 1995) and Southeast Pacific ODP Sites 1236 and 1237; (d) comparison of δ^{13}C profiles in central Equatorial Pacific DSDP Site 574 (*C. wuellerstorfi* and *C. mundulus* values from Pisias et al. (1985)), western Equatorial Pacific ODP Site 806 and Southeast Pacific ODP Site 1236. Increasing δ^{13}C contrast between intermediate and deep water sites after ~13.7–13.6 Ma supports relative "aging" of Equatorial and South Pacific deep water masses. CM6 indicates the last and most prominent δ^{13}C maximum of the "Monterey Excursion".

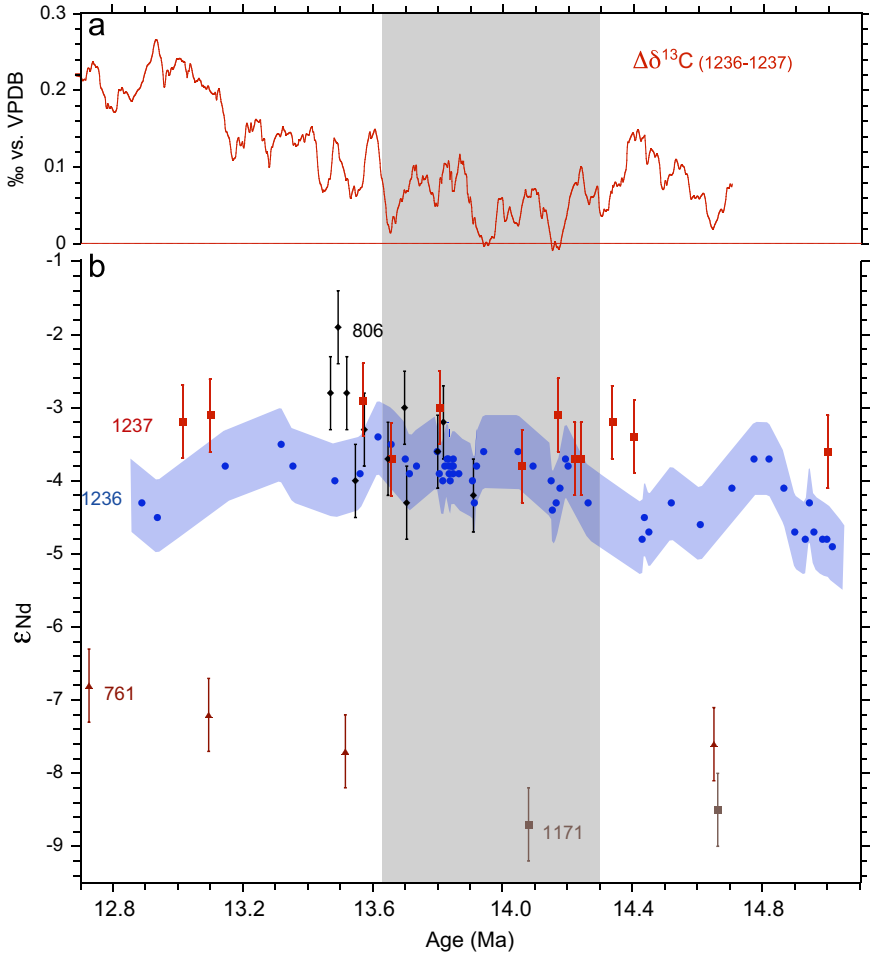

Fig. 5. (a) δ^{13}C gradient between Sites 1236 and 1237. Interpolated 20 pt smoothed δ^{13}C curves were re-sampled in 1 kyr intervals. $\Delta\delta^{13}$C data prior to 14.7 Ma are unreliable due to low resolution of the Site 1237 record and are not included. (b) The Nd isotope composition in ODP Sites 761, 806, 1171, 1236 and 1237 demonstrates progressive mixing of southern water masses with more radiogenic northerly sourced waters in the Pacific Ocean. Comparison of $\Delta\delta^{13}$C and Nd isotope data in Sites 1236 and 1237 reveals that Southeast Pacific intermediate and deep water masses were relatively homogenous between ~14.3 and 13.6 Ma, but increasingly diverged after 13.6 Ma.

2007), show a prominent 100 kyr eccentricity rhythm. This is particularly evident between 15 and 14.7 Ma and between 14 and 12.7 Ma, when δ^{18}O and Log(Mn/Ca) varied in anti-phase, indicating that eccentricity-paced carbonate dissolution cycles occurred during warmer intervals (Fig. 6). In contrast, δ^{18}O and Log(Mn/Ca) exhibit only a broad anti-phase variability without any distinct eccentricity beat between 14.7 and 14 Ma, which corresponds to a period of low 100 kyr eccentricity forcing and high amplitude variability in the 41 kyr obliquity cycle (Laskar et al., 2004). The 100 kyr beat is also imprinted on the benthic δ^{13}C records (Figs. 3 and 6), supporting that deep water ventilation deteriorated (δ^{13}C decreases) during warmer periods (δ^{18}O decreases) at high eccentricity (Holbourn et al., 2005, 2007). Other salient features of the Log(Mn/Ca) record are the marked increase in amplitude variations and the shift to substantially lower values during colder intervals (δ^{18}O maxima) between 13.9 and 12.7 Ma, following the major pulse of Antarctic ice expansion and global cooling at ~13.9 Ma (Fig. 6).

The total number of benthic foraminifers and the number of *Cibicidoides* spp. show marked increases in numbers after 13.9 Ma, following an initial transient increase at 14.3–14.2 Ma that coincided with a δ^{18}O increase (Fig. 6). As sedimentation rates approximately doubled after 13.9 Ma (Holbourn et al., 2007), benthic foraminiferal accumulation rates (not shown) exhibit even more pronounced increases between ~13.9 and 12.7 Ma. After 13.9 Ma, foraminiferal abundances display a marked 100 kyr beat, varying in phase with δ^{18}O and in antiphase with Log(Mn/Ca), which is consistent with increased bottom water ventilation and an intensified biological pump during colder intervals. The ratios between benthic and planktic foraminifers do not vary markedly after 13.9 Ma, supporting that foraminiferal abundances were primarily controlled by organic export fluxes to the seafloor rather than by changes in carbonate preservation. The higher abundances of *Cibicidoides* spp. during glacials provide an additional useful ventilation proxy, given that this taxon is known to consist mainly of suspension feeders that prefer well ventilated bottom water conditions (Mackensen et al., 1995).

7. Intensification of Pacific MOC following Antarctic glaciation at ~13.9 Ma

Comparison of δ^{13}C profiles at Southeast Pacific Sites 1236 and 1237, equatorial Pacific Sites 806, 574 and Southwest Pacific Sites 588 and 590 reveals a major change in Pacific intermediate and deep water circulation following the glacial expansion at ~13.9 Ma (Fig. 4, Supplementary Fig. S1). The δ^{13}C values exhibit an increasing offset between shallower and deeper locations, as δ^{13}C becomes more depleted at the deeper Sites 1237 (Southeast Pacific Ocean), 806 and 574 (Equatorial Pacific Ocean) and 588

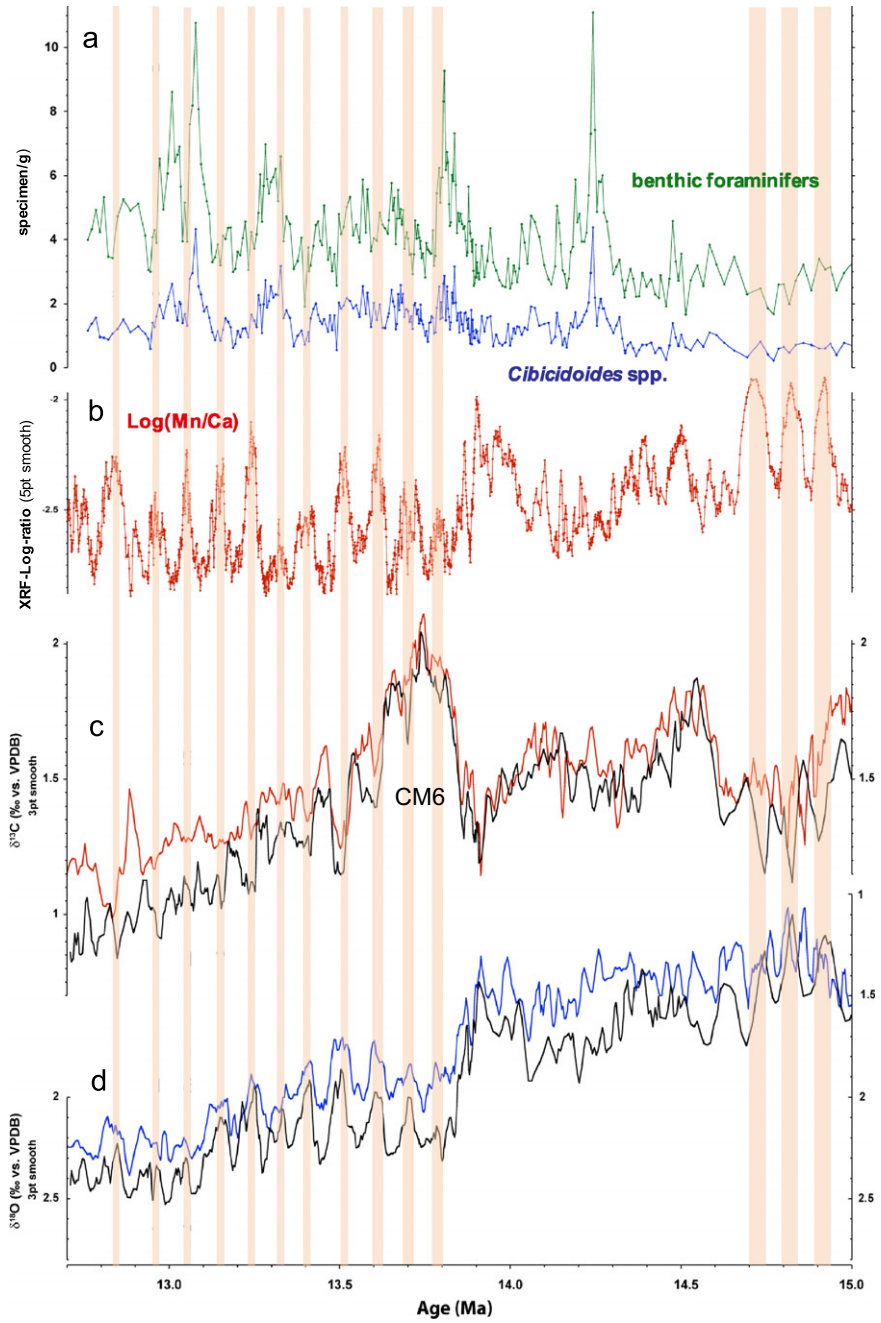

Fig. 6. Deep water ventilation proxy records (XRF Log(Mn/Ca) and benthic foraminiferal $\delta^{13}C$) in ODP Site 1237 display a strong 100 kyr beat at 15–14.6 Ma and at 13.9–12.7 Ma (highlighted by orange bars), indicating that deep water ventilation deteriorated during warmer intervals; (a) Benthic foraminiferal and *Cibicidoides* spp. abundances vary in phase with $\delta^{18}O$ and in antiphase with Log(Mn/Ca); (b) XRF scanning Log(Mn/Ca); (c) Comparison of (3 pt) smoothed $\delta^{13}C$ profiles in ODP Sites 1236 (red) and 1237 (black) reveals progressive development of $\delta^{13}C$ offset between shallower and deeper water masses after 13.6 Ma. CM6 indicates the last and most prominent $\delta^{13}C$ maximum of the "Monterey Excursion"; (d) Comparison of (3 pt) smoothed $\delta^{18}O$ profiles in ODP Sites 1236 (blue) and 1237 (black).

(Southwest Pacific Ocean) during CM6, implying that this change represents an ocean-wide feature. The divergence in $\delta^{13}C$ between deeper and shallower sites appears to have started somewhat earlier at ~13.8 Ma in the Southwest Pacific Ocean, in contrast to ~13.6 Ma in the Southeast and Equatorial Pacific Ocean, possibly reflecting asymmetric northward spreading of AAIW. However, the relative timing of the change is difficult to ascertain in the Southwest Pacific Ocean due to the low temporal resolution of the Site 590 isotope record. In contrast, the 1236 and 1237 Nd and $\delta^{13}C$ data indicate a vertically more homogeneous water mass structure in the Southeast tropical Pacific between 14.3 and 13.6 Ma (Fig. 5).

We attribute the intensified $\delta^{13}C$ gradient between Pacific intermediate and deep waters to an enhancement of the MOC following the onset of permanent Antarctic glaciation and global cooling after 13.9 Ma (Fig. 7). As a result, the deeper Equatorial and Southeast Pacific sites became increasingly affected by the return southward PCW flow (more depleted $\delta^{13}C$), whereas the shallower Southeast Pacific Site 1236 remained in the mixing zone of AAIW and PCW (enriched $\delta^{13}C$). Although the Site 1236 Nd isotope data do not provide clear evidence for increased advection of AAIW into the subtropical Southeast Pacific Ocean (~20°S), most likely because the difference between the Nd isotope end member signatures was too small, northward expansion of AAIW into the

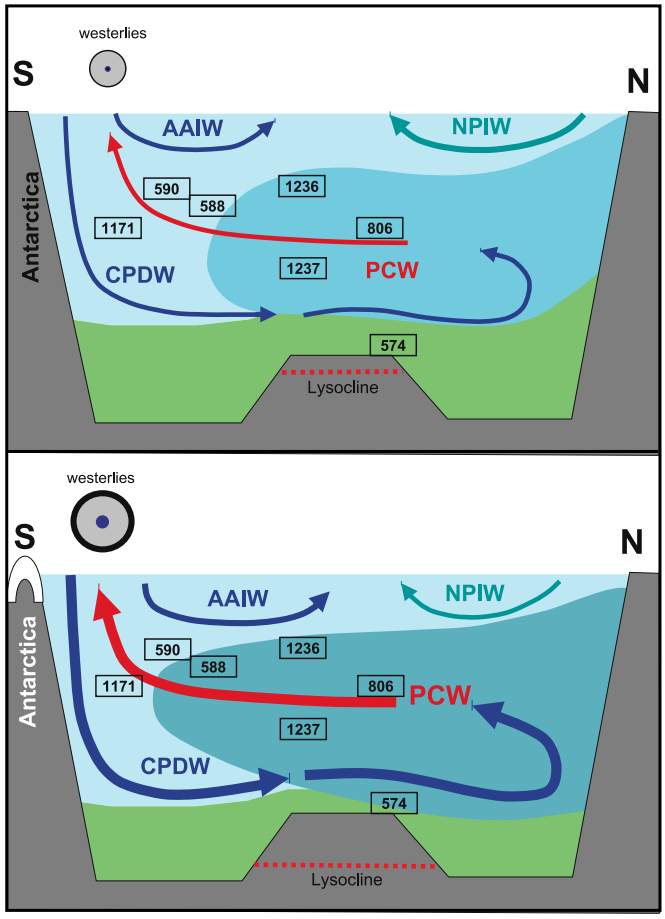

Fig. 7. Summary cartoons of Pacific circulation changes following Antarctic ice-sheet expansion after 13.9 Ma. CPDW: Circumpolar Deep Water; AAIW: Antarctic Intermediate Water; PCW: Pacific Central Water; NPIW: North Pacific Intermediate Water. Ventilation of the deep Pacific Ocean improved after 13.9 Ma, as increased production of CPDW and AAIW equivalent waters promoted enhanced entrainment of PCW into the wind-driven ocean circulation, favoring a more vigorous "estuarine" circulation. Changes in line thickness between panels relate to flow rates and strength of Pacific meridional overturning. Darker blue shading of the water column indicates higher concentration of regenerated nutrients. (For interpretation of the references to color in this figure legend, the reader is referred to the web version of this article.)

Southwest Pacific Ocean is supported by the marked $\delta^{13}C$ divergence in Sites 588, 590 and 591 (~30–35°S) after 13.8 Ma (Fig. 4; Flower and Kennett, 1995). The gradual increase in the $\delta^{18}O$ gradient (from 0.9‰ to 1.2‰ between ~13.8 and 13.1 Ma) between the shallow Site 590, mainly bathed in AAIW, and the deep Site 1237 bathed in PCW further indicates increasing density (cooling) of PCW after 13.8 Ma (Fig. 4).

The 1237 XRF Log(Mn/Ca) and benthic foraminiferal data additionally provide evidence that southern hemisphere cooling after 13.9 Ma promoted an amelioration in Pacific deep water ventilation (Fig. 6). The Log(Mn/Ca) curve exhibits a shift toward more negative values, indicating improved carbonate preservation and deepening of the lysocline after 13.9 Ma, in particular during colder climate phases. Benthic foraminifers, in particular suspension feeders (*Cibicidoides* spp.), increase markedly in this deep site after 13.9 Ma, supporting more vigorous bottom currents and improved deep water ventilation. Our results suggest that strengthening of the MOC occurred as a direct response to Antarctic glacial expansion after 13.9 Ma, fostering a general improvement in Pacific ventilation with development of a steeper $\delta^{13}C$ gradient between Pacific intermediate and deep waters during CM6 (Figs. 4 and 6). A plausible scenario is that southern hemisphere cooling after 13.9 Ma led to a steeper latitudinal temperature gradient with stronger westerlies promoting intensification of the Antarctic Circumpolar Current. Increased upwelling in the Southern Ocean in turn stimulated formation of deep and intermediate waters, thus strengthening overturning and encouraging a more vigorous "estuarine" circulation in the Pacific Ocean (Fig. 7). Seasonal formation of sea ice and local development of ice shelves along the Antarctic margin following ice expansion would have additionally amplified production of cold, dense deep and intermediate waters.

A decreasing trend in $\delta^{13}C$ is evident in Pacific Sites 574, 588, 590, 806, 1236 and 1237 between 13.5 and 12.7 Ma following the last carbon maximum (CM6) of the "Monterey Excursion" (Figs. 3, 4 and 6). This long-lasting trend is also present at Site 1171, located close to the source area of South Pacific intermediate and deep waters (Shevenell et al., 2004, 2008), implying that it cannot be attributed to a long-term decrease in Pacific ventilation or increased advection of $\delta^{13}C$ depleted water masses originating from the North Pacific Ocean. In fact, the long-term $\delta^{13}C$ decline in Pacific benthic isotope records at the end of CM6 after 13.5 Ma is also characteristic of intermediate and deep water records from the Indian, Atlantic and Pacific Oceans (Woodruff and Savin, 1989; Wright et al., 1992; Wright and Miller, 1993), thus representing a global feature probably related to a re-adjustment of the global carbon cycle after the end of the "Monterey Excursion". The small variability in the 1236 and 1237 Nd isotope signatures between 15 and 12.7 Ma further supports that the decreasing $\delta^{13}C$ trend does not represent a gradual shift in the provenance of Pacific water masses after 13.5 Ma.

8. Eccentricity-paced ventilation cycles

A striking feature of the 1237$\delta^{18}O$, $\delta^{13}C$, XRF Log(Mn/Ca) and benthic foraminiferal abundance records is the prominent 100 kyr cyclicity that is superimposed on long-term circulation trends (Fig. 6). This is particularly evident between 13.9 and 12.7 Ma, when ventilation proxy records ($\delta^{13}C$, XRF Log(Mn/Ca) and benthic foraminiferal abundances) indicate that deep water ventilation deteriorated and carbonate dissolution increased during warm climate modes at high eccentricity, whereas carbonate preservation improved during colder phases (low eccentricity). Coarse fraction data in Site 1237 additionally provide evidence for enhanced carbonate preservation during colder periods corresponding to low eccentricity after 13.9 Ma (Holbourn et al., 2005, 2007). However, middle Miocene circulation differed markedly from the late Pleistocene scenario, when enhanced NADW production drove a more vigorous overturning and the deep Atlantic and Southern Oceans (and possibly the Pacific Ocean) became better ventilated during interglacials, whereas ventilation weakened during glacials due to a decline in NADW and increased contribution of Glacial North Atlantic Intermediate Water (Galbraith et al., 2007; Anderson et al., 2009; Sigman et al., 2010). Furthermore, the mechanisms controlling deep water formation and overturning rates probably varied significantly before and after the onset of permanent ice cover in Antarctica after 13.9 Ma, due to changing boundary conditions.

Firstly, NADW formation was probably not the main driver of the global thermohaline circulation during the middle Miocene, as the northern hemisphere was relatively warm with a more reduced ice cover than in the late Pleistocene. Recent modeling simulations (Butzin et al., 2011) additionally indicated that a relatively deep (> 0.5 km) Central American Seaway during the middle Miocene would have favored net export of water from the Pacific to the Atlantic, thereby reducing the salinity contrast between the two oceans and inhibiting NADW formation.

Secondly, the middle Miocene ice cover over East and West Antarctica was probably less extensive than during the late Pleistocene, and fluctuated considerably between warmer and colder phases, even following the 13.9 Ma glacial expansion (Lewis et al., 2006; Haywood et al., 2008). It is therefore unlikely that extensive ice shelves, which inhibited downwelling and deep water production during the last glacial maximum (Anderson et al., 2009; Sigman et al., 2010), developed around Antarctica following middle Miocene ice growth. However, sinking of colder, denser water probably intensified along the margins of Antarctica during intervals of glacial expansion, as the westerlies increased in strength due to the steeper latitudinal temperature gradient, promoting more vigorous upwelling in the Southern Ocean. The Pacific Ocean became better ventilated during colder episodes of glacial expansion, when deep water formation increased and northward export of southern-sourced waters intensified. Therefore, our proxy data suggest that eccentricity-paced variations of a more extended Antarctic ice cover after 13.9 Ma led to enhanced variability in intermediate and deep water production in the Southern Ocean, thus exerting a major control on the strength of the Pacific MOC.

9. Comparison with modeling predictions

Modeling studies of Miocene ocean circulation have mainly focused on the response of the MOC to gateway restriction or closure (e.g. Heinze and Crowley, 1997; Nisancioglu et al., 2003; Motoi et al., 2005; von der Heydt and Dijkstra, 2006; Butzin et al., 2011). Experiments have investigated, in particular, how changes in the depth of the Central American Seaway and its eventual closure may have impacted inter-ocean exchange and rates of overturning. Predicted outcomes, however, vary considerably in terms of the flow direction and depth, repercussion on deep water production and inter-ocean heat and salt exchange. Although most studies (except for that of Nisancioglu et al. (2003)) support a net deep water export from the Pacific Ocean into the Atlantic Ocean through a relatively deep Central American Seaway, there is considerable divergence concerning the rates of inter-ocean flow and the main locations of deep water formation. Especially controversial are the timing for the onset of NADW production and the role that NADW may have played within the global circulation system during the Miocene.

The model sensitivity study of Butzin et al. (2011), which investigated the evolution of ocean circulation with various seaway configurations, concluded that the Central American Seaway played a crucial role during the Miocene. Simulations with a seaway depth >0.5 km, a realistic scenario for the middle Miocene (Duque-Caro, 1990; Coates et al., 2003), indicated increased production of deep and intermediate waters in the South Pacific, linked to cooling of Antarctica during the middle Miocene (Fig. 3 in Butzin et al. (2011)). Modeling experiments showed that a relatively deep (>0.5 km) and narrow Central American Seaway favored water export from the Pacific to the Atlantic Oceans, and inhibited substantial production of NADW. This in turn led to the establishment of a deep southward return flow along the South American Atlantic coast, eventually merging into the Antarctic Circumpolar Current (Fig. 7 in Butzin et al. (2011)). In contrast, the export flow from the Pacific Ocean into the Atlantic Ocean and the southward return branch from the tropical Atlantic to the Southern Ocean weakened substantially when the Antarctic continent was warmer.

Our data do not support that deep water production in the North Pacific (von der Heydt and Dijkstra, 2006) or westward transport of NADW through the Central American Seaway (Nisancioglu et al., 2003) had a major impact on the Pacific MOC during the middle Miocene. In contrast, our results suggest that Pacific deep and intermediate waters predominantly originated from the Southern Ocean and that the MOC strengthened substantially following high latitude cooling and Antarctic ice-sheet expansion. This interpretation is overall more consistent with modeling outcomes of Miocene Pacific MOC in Butzin et al. (2011). Increased NADW production and enhanced export to the Southern Ocean may have accompanied middle Miocene global cooling. However, such changes are not readily detectable in our data sets, as the deep water originating from the North Atlantic would have lost its original Nd and δ^{13}C signatures during the long southward transit and through mixing with Southern Ocean waters.

10. Conclusion

We used a range of proxies including δ^{13}C, Nd isotopes, benthic foraminiferal abundances and XRF-scanner derived elemental data in well dated sedimentary successions to monitor changes in Pacific water masses and MOC strength during the middle Miocene transition into a colder climate mode following Antarctic ice-sheet expansion. Nd isotopes reveal that Pacific water masses became progressively more radiogenic northward, much as today, and that the provenance of intermediate and deep water masses did not change markedly in the subtropical Southeast Pacific Ocean between 15 and 12.7 Ma. Both $\Delta\delta^{13}$C and Nd isotope data document a vertically better mixed water column in the Southeast Pacific Ocean between 14.3 and 13.6 Ma. Benthic foraminifers and Log(Mn/Ca) data indicate an ocean-wide improvement in deep water ventilation and strengthening of the MOC following major ice-sheet expansion at $\sim$13.9 Ma. We attribute the sharper δ^{13}C contrast between Pacific deep and intermediate water masses between $\sim$13.6 and 12.7 Ma to increased advection of δ^{13}C depleted deep waters into the equatorial and South Pacific Ocean, due to more vigorous entrainment of PCW into the wind-driven circulation and strengthening of the MOC. In contrast, the shallower South Pacific sites remained within the mixing zone of AAIW and PCW or became increasingly affected by northward incursion of AAIW. Eccentricity-paced variations of an expanded Antarctic ice sheet after 13.9 Ma drove marked changes in intermediate and deep water production during warmer and colder climate phases. The deep Pacific Ocean remained poorly ventilated during warmer intervals (high eccentricity), whereas increased intermediate and deep water formation during colder periods (low eccentricity) resulted in a more vigorous MOC, improved ventilation and enhanced carbonate preservation. The long-term δ^{13}C decline in Pacific intermediate and deep water sites between 13.5 and 12.7 Ma reflects a global trend, probably related to a re-adjustment response of the global carbon cycle following the "Monterey Excursion". Increases in the preformed nutrient content at sites of intermediate and deep water formation in the Southern Ocean may have additionally accentuated this long-term trend.

Acknowledgments

This research used samples provided by the Ocean Drilling Program (ODP) and was funded by the Deutsche Forschungsgemeinschaft (Grant Ku649/27). We thank Folkmar Hauff for smooth operation of the TIMS facility at GEOMAR, Ulla Röhl for advice regarding XRF scanning and Nils Andersen for isotope measurements. We are also very grateful to the editor Gideon Henderson and to two anonymous referees for insightful, constructive comments.

Appendix A. Supporting information

Supplementary data associated with this article can be found in the online version at http://dx.doi.org/10.1016/j.epsl.2013.01.020.

References

Abels, H.A., Hilgen, F.J., Krijgsman, W., Kruk, R.W., Raffi, I., Turco, E., Zachariasse, W.J., 2005. Long-period orbital control on middle Miocene global cooling: integrated stratigraphy and astronomical tuning of the Blue Clay Formation on Malta. Paleoceanography 20, PA4012, http://dx.doi.org/10.1029/2004PA001129.

Albarède, F., Goldstein, S.L., 1992. World map of Nd isotopes in sea-floor ferromanganese deposits. Geology 20, 761–763.

Albarède, F., Goldstein, S.L., Dautel, D., 1997. The neodymium isotopic composition of manganese nodules from the Southern and Indian Oceans, the global oceanic neodymium budget, and their bearing on deep ocean circulation. Geochim. Cosmochim. Acta 61, 1277–1291.

Amakawa, H., Sasaki, K., Ebihara, M., 2009. Nd isotopic composition in the central North Pacific. Geochim. Cosmochim. Acta 73, 4705–4719.

Anderson, R.F., Ali, S., Bradtmiller, L.I., Nielsen, S.H.H., Fleisher, M.Q., Anderson, B.E., Burckle, L.H., 2009. Wind-driven upwelling in the southern ocean and the deglacial rise in atmospheric CO_2. Science 323, 1443–1448.

Barrat, J.A., Keller, F., Amossé, J., 1996. Determination of rare earth elements in sixteen silicate reference samples by ICP-MS after Tm addition and ion exchange separation. Geostand. Newsl. 20, 133–139.

Bayon, G., German, C.R., Boella, R.M., Milton, J.A., Taylor, R.N., Nesbitt, R.W., 2002. An improved method for extracting marine sediment fractions and its application to Sr and Nd isotopic analysis. Chem. Geol. 187, 170–199.

Broecker, W.S., Clark, E., Hajdas, I., Bonani, G., 2004. Glacial ventilation rates for the deep Pacific Ocean. Paleoceanography 19, PA2002, http://dx.doi.org/10.1029/2003PA000974.

Broecker, W.S., Clark, E., Barker, S., 2008. Near constancy of the Pacific Ocean surface to mid-depth radiocarbon-age difference over the last 20 kyr. Earth Planet. Sci. Lett. 274, 322–326.

Butzin, M., Lohmann, G., Bickert, T., 2011. Miocene ocean circulation inferred from marine carbon cycle modeling combined with benthic isotope records. Paleoceanography 26, PA1203, http://dx.doi.org/10.1029/2009PA001901.

Carter, P., Vance, D., Hillenbrand, C.D., Smith, J.A., Shoosmith, D.R., 2012. The neodymium isotopic composition of waters masses in the eastern Pacific sector of the Southern Ocean. Geochim. Cosmochim. Acta 79, 41–59.

Coates, A.G., Aubry, M.-P., Berggren, W.A., Collins, L.S., Kunk, M., 2003. Early Neogene history of the Central American arc from Bocas del Toro, western Panama. Geol. Soc. Am. Bull. 115, 271–287.

Cohen, A.S., O'Nions, R.K., Siegenthaler, R., Griffin, W.L., 1988. Chronology of the pressure–temperature history recorded by a granulite terrain. Contrib. Mineral. Petrol. 98, 303–311.

Cramer, B.S., Toggweiler, J.R., Wright, J.D., Katz, M.E., Miller, K.G., 2009. Ocean overturning since the Late Cretaceous: inferences from a new benthic foraminiferal isotope compilation. Paleoceanography 24, PA4216, http://dx.doi.org/10.1029/2008PA001683.

Duque-Caro, H., 1990. Neogene stratigraphy, paleoceanography and paleobiogeography in northwest South America and the evolution of the Panama seaway. Palaeogeogr. Palaeoclimatol. Palaeoecol. 77, 203–234.

Elmore, A.C., Piotrowski, A.M., Wright, J.D., Scrivner, A.E., 2011. Testing the extraction of past seawater Nd isotopic composition from North Atlantic deep sea sediments and foraminifera. Geochem. Geophys. Geosyst. 12, Q09008, http://dx.doi.org/10.1029/2011GC003741.

Emile-Geay, J., et al., 2003. Warren revisited: atmospheric freshwater fluxes and why is no deep water formed in the North Pacific. J. Geophys. Res. 108, 3178, http://dx.doi.org/10.1029/2001JC001058.

Flower, B.P., Kennett, J.P., 1993. Middle Miocene ocean-climate transition: high resolution oxygen and carbon isotopic records from DSDP Site 588A, southwest Pacific. Paleoceanography 8, 811–843.

Flower, B.P., Kennett, J.P., 1995. Middle Miocene deep water paleoceanography in the southwest Pacific: relations with East Antarctic ice sheet development. Paleoceanography 10, 1095–1112.

Frank, M., 2002. Radiogenic isotopes: tracers of past ocean circulation and erosional input. Rev. Geophys. 40 (1), 1001, http://dx.doi.org/10.1029/2000RG000094.

Frank, M., Reynolds, B.C., O'Nions, R.K., 1999. Nd and Pb isotopes in Atlantic and Pacific water masses before and after closure of the Panama gateway. Geology 27, 1147–1150.

Frank, M., Whiteley, N., Kasten, S., Hein, J.R., O'Nions, K., 2002. North Atlantic Deep water export to the Southern Ocean over the past 14 Myr: evidence from Nd and Pb isotopes in ferromanganese crusts. Paleoceanography 17, 1022, http://dx.doi.org/10.1029/2000PA000606.

Galbraith, et al., 2007. Carbon dioxide release from the North Pacific abyss during the last deglaciation. Nature 449, 890–894.

Grasse, P., Stichel, T., Stumpf, R., Stramma, L., Frank, M., 2012. The distribution of neodymium isotopes and concentrations in the Eastern Equatorial Pacific: water mass advection versus particle exchange. Earth Planet. Sci. Lett. 353-354, 198–207.

Gutjahr, M., Frank, M., Stirling, C.H., Klemm, V., van de Flierdt, T., Halliday, A.N., 2007. Reliable extraction of a deepwater trace metal isotope signal from Fe–Mn oxyhydroxide coatings of marine sediments. Chem. Geol. 242, 351–370.

Haywood, A.M., et al., 2008. Middle Miocene to Pliocene history of Antarctica and the Southern Ocean. In: Fabio Florindo, Martin Siegert (Eds.), Antarctic Climate Evolution, Developments in Earth and Environmental Science, vol. 8. ISBN: 978-0-444- 52847-6, pp. 401–463. Elsevier. The Netherlands.

Heinze, C., Crowley, T.J., 1997. Sedimentary response to ocean gateway circulation changes. Paleoceanogr 12 (6), 742–754.

Holbourn, A.E., Kuhnt, W., Simo, J.A., Li, Q., 2004. Middle Miocene isotope stratigraphy and paleoceanographic evolution of the northwest and southwest Australian margins (Wombat Plateau and Great Australian Bight). Palaeogeogr. Palaeoclimatol. Palaeoecol. 208, 1–22.

Holbourn, A., Kuhnt, W., Schulz, M., Erlenkeuser, H., 2005. Impacts of orbital forcing and atmospheric carbon dioxide on Miocene ice-sheet expansion. Nature 438, 483–487.

Holbourn, A., Kuhnt, W., Schulz, M., Flores, J., Andersen, N., 2007. Orbitally-paced climate evolution during the middle Miocene "Monterey" carbon-isotope excursion. Earth Planet. Sci. Lett. 261, 534–550.

Horikawa, K., Martin, E.E., Asahara, Y., Sagawa, T., 2011. Limits on conservative behavior of Nd isotopes in seawater assessed from analysis of fish teeth from Pacific core tops. Earth Planet. Sci. Lett. 310, 119–130.

Jacobsen, S.B., Wasserburg, G.J., 1980. Sm–Nd isotopic evolution of chondrites. Earth Planet. Sci. Lett. 50, 139–155.

Katz, M.E., Cramer, B.S., Toggweiler, J.R., Esmay, G., Liu, C., Miller, K.G., Rosenthal, Y., Wade, B.S., Wright, J.D., 2011. Impact of Antarctic circumpolar current development on late Paleogene ocean structure. Science 332, 1076, http://dx.doi.org/10.1126/science.1202122.

Kiefer, T., 2010. When still waters ran deep. Science 329, 290, http://dx.doi.org/10.1126/science.1192295.

Kroenke, L.W., Berger, W.H., Janacek, T.R. (Eds.), 1991. Proceedings of the Ocean Drilling Program, Initial Reports, 130. Ocean Drilling Program, College Station, Texas.

Kroopnick, P.M., 1985. The distribution of ^{13}C of ΣCO_2 in the world oceans. Deep Sea Res. 32, 57–84.

Lacan, F., Jeandel, C., 2001. Tracing Papua New Guinea imprint on the central Equatorial Pacific Ocean using neodymium isotopic compositions and Rare Earth Element patterns. Earth Planet. Sci. Lett. 186, 497–512.

Laskar, J., et al., 2004. A long term numerical solution for the insolation quantities of the Earth. Astron. Astrophys. 428, 261–285.

Le Fèvre, B., Pin, C., 2005. A straightforward separation scheme for concomitant Lu–Hf and Sm–Nd isotope ratio and isotope dilution analysis. Anal. Chim. Acta 543, 209–221.

Lewis, A.R., Marchant, D.R., Kowalewski, D.E., Baldwin, S.L., Webb, L.E., 2006. The age and origin of the Labyrinth, western Dry Valleys, Antarctica: evidence for extensive middle Miocene subglacial floods and freshwater discharge to the Southern Ocean. Geology 34, 513–516.

Ling, H.-F., Burton, K.W., O'Nions, R.K., Kamber, B.S., von Blanckenburg, F., Gibb, A.J., Hein, J.R., 1997. Evolution of Nd and Pb isotopes in Central Pacific seawater from ferromanganese crusts. Earth Planet. Sci. Lett. 146, 1–12.

Ling, H.-F., Jiang, S.-Y., Frank, M., Zhou, H.-Y., Zhou, F., Lu, Z.-L., Chen, X.-M., Jiang, Y.-H., Ge, C.D., 2005. Differing controls over the Cenozoic Pb and Nd isotope evolution of deepwater in the central North Pacific Ocean. Earth Planet. Sci. Lett. 232, 345–361.

Mackensen, A., Schmiedl, G., Harloff, J., Giese, M., 1995. Deep-sea foraminifera in the South Atlantic Ocean: ecology and assemblage generation. Micropaleontology 41, 342–358.

Marchitto, T., et al., 2007. Marine radiocarbon evidence for the mechanism of deglacial atmospheric CO_2 rise. Science 316, 1456–1459.

Martin, E.E., Scher, H.D., 2004. Preservation of seawater Sr and Nd isotopes in fossil fish teeth: bad news and good news. Earth Planet. Sci. Lett. 220, 25–39.

Martin, E.E., Blair, S.W., Kamenov, G.D., Scher, H.D., Bourbon, E., Basak, C., Newkirk, D.N., 2010. Extraction of Nd isotopes from bulk deep sea sediments for paleoceanographic studies on Cenozoic time scales. Chem. Geol. 269, 414–431.

Mayer, L., Theyer, F., et al., 1985. Initial Reports. DSDP, 85, Washington (US Government Printing Office).

Mix, A.C., Tiedemann, R., Blum, P., et al., 2003. Proceedings of ODP, Initial Reports, 202, College Station, TX (Ocean Drilling Program), http://dx.doi.org/10.2973/odp.proc.ir.202.2003.

Motoi, T., Chan, W.-L., Minobe, S., Sumata, H., 2005. North Pacific halocline and cold climate induced by Panamanian Gateway closure in a coupled ocean-atmosphere GeM. Geophys. Res. Lett. 32, Ll0618 doi:l0.1029/2005GL022844.

Newkirk, D.R., Martin, E.E., 2009. Circulation through the Central American Seaway during the Miocene carbonate crash. Geology 37, 87–90.

Nisancioglu, K., Raymo, M.E., Stone, P.H., 2003. Reorganization of Miocene deep water circulation in response to the shoaling of the Central American Seaway. Paleoceanography 18, 1006, http://dx.doi.org/10.1029/2002PA000767.

Piepgras, D.J., Jacobsen, S.B., 1988. The isotopic composition of neodymium in the North Pacific. Geochim. Cosmochim. Acta 52, 1373–1381.

Piotrowski, A.M., Goldstein, S.L., Hemming, S.R., Fairbanks, R.G., 2005. Temporal relationships of carbon cycle and ocean circulation at glacial boundaries. Science 307, 1933–1938.

Pisias, N.G., Shackleton, N.J., Hall, M.A., 1985. Stable isotope and calcium carbonate records from hydraulic piston cored Hole 574A: high-resolution records from the Middle Miocene. In: Mayer, L., Theyer, F., et al., Initial Reports DSDP, 85, Washington (US Government Printing Office), pp. 735–748.

Poore, H.R., Samworth, R., White, N.J., Jones, S.M., McCave, I.N., 2006. Neogene overflow of northern component water at the Greenland–Scotland ridge. Geochem. Geophys. Geosyst. 7, Q06010, http://dx.doi.org/10.1029/2005GC001085.

Reid, J.L., 1986. On the total geostrophic circulation of the South Pacific Ocean: flow patterns, tracers and transports. Prog. Oceanogr. 16, 1–61.

Reid, J.L., 1997. On the total geostrophic circulation of the Pacific Ocean: flow patterns, tracers, and transports. Prog. Oceanogr. 39, 263–352.

Roberts, N.L., Piotrowski, A.M., McManus, J.F., Keigwin, L.D., 2009. Synchronous deglacial overturning and water mass source changes. Science 327, 75–78.

Robinson, L.F., et al., 2005. Radiocarbon variability in the western North Atlantic during the last deglaciation. Science 310, 1469–1473.

Rutberg, R.L., Hemming, S.R., Goldstein, S.L., 2000. Reduced North Atlantic Deep Water flux to the glacial Southern Ocean inferred from neodymium isotope ratios. Nature 405, 935–938.

Savin, S.M., Douglas, R.G., Stehli, F.G., 1975. Tertiary marine paleotemperatures. Geol. Soc. Am. Bull. 86, 1499–1510.

Scher, H.D., Martin, E.E., 2008. Oligocene deep water export from the North Atlantic and the development of the Antarctic Circumpolar Current examined with neodymium isotopes. Paleoceanography 23, PA1205, http://dx.doi.org/10.1029/2006PA001400.

Shackleton N.J. and Kennett, J.P., 1975. Paleotemperature history of the Cenozoic and the initiation of Antarctic glaciation: oxygen and carbon analyses in DSDP Sites 277, 279, and 281. Initial Reports of the Deep Sea Drilling Project, 29, pp. 743–755.

Shevenell, A.E., Kennett, J.P., Lea, D.W., 2004. Middle Miocene Southern Ocean cooling and Antarctic cryosphere expansion. Science 305, 1766–1770.

Shevenell, A.E., Kennett, J.P., 2004. Paleoceanographic change during the middle Miocene climate revolution: an Antarctic stable isotope perspective. In: Exon, N., Kennett, J.P., Malone, M. (Eds.), The Cenozoic Southern Ocean: Tectonics, Sedimentation and Climate Change between Australia and Antarctica. Geophysical Monograph Series 151. American Geophysical Union, Washington, DC, pp. 235–252.

Shevenell, A.E., Kennett, J.P., Lea, D.W., 2008. Middle Miocene ice sheet dynamics, deep sea temperatures, and carbon cycling: a Southern Ocean perspective. Geochem. Geophys. Geosyst. 9, Q02006, http://dx.doi.org/10.1029/2007GC001736.

Sigman, D.M., Hain, M.P., Haug, G.H., 2010. The polar ocean and glacial cycles in atmospheric CO_2 concentration. Nature 466, 47–55.

Sikes, E.L., Samson, C.R., Guilderson, T.P., Howard, W.R., 2000. Old radiocarbon ages in the southwest Pacific Ocean during the last glacial period and deglaciation. Nature 405, 555–559.

Stichel, T., Frank, M., Rickli, J., Haley, B.A., 2012. The hafnium and neodymium isotope composition of seawater in the Atlantic sector of the Southern Ocean. Earth Planet. Sci. Lett. 317–318, 282–294.

Talley, L.D., 1993. Distribution and formation of North Pacific Intermediate Water. J. Phys. Oceanogr. 23, 517–537.

Talley, L.D., 1997. North Pacific intermediate water transports in the mixed water region. J. Phys. Oceanogr. 27, 1795–1803.

Talley, L.D., 1999. Some aspects of ocean heat transport by the shallow, intermediate and deep overturning circulations. In: Clark, U., Webb, S., Keigwin, D. (Eds.), Mechanisms of Global Climate Change at Millenial Time Scales. Geophysical Monograph Series 112. American Geophysical Union, pp. 1–22.

Talley, L.D., 2007. Hydrographic atlas of the World Ocean Circulation Experiment (WOCE). In: Sparrow, M., Chapman, P., Gould, J. (Eds.), Pacific Ocean, vol. 2. International WOCE Project Office, Southampton, U.K., ISBN: 0-904175-54-5.

Tanaka, T., Togashi, S., Kamioka, H., Amakawa, H., Kagami, H., Hamamoto, T., Yuhara, M., Orihashi, Y., Yoneda, S., Shimizu, H., Kunimaru, T., Takahashi, K., Yanagi, T., Nakano, T., Fujimaki, H., Shinjo, R., Asahara, Y., Tanimizu, M., Dragusanu, C., 2000. JNdi-1: a neodymium isotopic reference in consistency with LaJolla neodymium. Chem. Geol. 168, 279–281.

Thomas, D.J., Via, R.K., 2007. Neogene evolution of Atlantic thermohaline circulation: perspective from Walvis Ridge, southeastern Atlantic Ocean. Paleoceanography 22, PA2212, http://dx.doi.org/10.1029/2006PA001297.

Tsuchiya, M., Talley, L.D., 1996. Water-property distributions along an eastern Pacific hydrographic section at 135°W. J. Mar. Res. 54, 541–564.

van de Flierdt, T., Frank, M., Halliday, A.N., Hein, J.R., Hattendorf, B., Günther, D., Kubik, P.W., 2004a. Deep and bottom water export from the Southern Ocean to the Pacific over the past 38 million years. Paleoceanography 19, PA1020, http://dx.doi.org/10.1029/2003PA000923.

van de Flierdt, T., Frank, M., Lee, D.-C., Halliday, A.N., Reynolds, B.C., Hein, J.R., 2004b. New constraints on the sources and behavior of neodymium and hafnium in seawater from Pacific Ocean ferromanganese crusts. Geochim. Cosmochim. Acta 68, 3827–3843.

Via, R.K., Thomas, D.J., 2006. Evolution of Atlantic thermohaline circulation: early Oligocene onset of deep-water production in the North Atlantic. Geology 34, 441–444.

von der Heydt, A., Dijkstra, H.A., 2006. Effect of ocean gateways on the global ocean circulation in the late Oligocene and early Miocene. Paleoceanography 21, PA1O11 doi:l0.1029/2005PA001149.

Warren, B., 1983. Why is no deepwater formed in the North Pacific? J. Mar. Res. 41, 327–347.

Woodruff, F., Savin, S., 1989. Miocene deepwater oceanography. Paleoceanography 4, 87–140.

Woodruff, F., Savin, S., 1991. Mid-Miocene isotope stratigraphy in the deep sea: high resolution correlations, paleoclimatic cycles, and sediment preservation. Paleoceanography 6, 755–806.

Wright, J.D., Miller, K.G., Fairbanks, R.G., 1992. Evolution of modern deepwater circulation: evidence from the late Miocene Southern Ocean. Paleoceanography 6, 275–290.

Wright, J.D., Miller, K.G., 1993. Southern Ocean Influences on Late Eocene to Miocene Deepwater Circulation. Antarctic Research Series, 60, pp. 1–25.

You, Y., 2003. The pathway and circulation of North Pacific Intermediate Water. Geophys. Res. Lett. 30, 2291, http://dx.doi.org/10.1029/2003GL018561.